Aerodynamic Analysis of Flapped Airfoil at High Angles of Attack

Conference Paper · January 2018

DOI: 10.2514/6.2018-0037

4 authors:

Hisham M. Shehata
Virginia Polytechnic Institute and State University
1 PUBLICATION **0** CITATIONS
SEE PROFILE

Mohamed Yehia Zakaria
Military Technical College
32 PUBLICATIONS **81** CITATIONS
SEE PROFILE

Ahmed A Hussein
Virginia Polytechnic Institute and State University
9 PUBLICATIONS **9** CITATIONS
SEE PROFILE

Muhammad R. Hajj
Virginia Polytechnic Institute and State University
273 PUBLICATIONS **2,678** CITATIONS
SEE PROFILE

AIAA SciTech Forum
8–12 January 2018, Kissimmee, Florida
2018 AIAA Aerospace Sciences Meeting

10.2514/6.2018-0037

Aerodynamic Analysis of Flapped Airfoil at High Angles of Attack

Hisham Shehata* , Mohamed Y. Zakaria† Ahmed Hussein* and Muhammad R. Hajj‡

The use of oscillatory actuation of the trailing edge for a rigid airfoil as a potential mechanism for control or performance improvement of flying vehicles was investigated. Aerodynamic analysis involved performing a wind tunnel testing of a NACA 0012 wing spanning the total width of the test section. The measurements were conducted at a Reynolds numbers of 21 x 10^3. The trailing edge of the airfoil is hinged at 75% of the chord length from the leading edge allowing dynamic variations in the effective angle of attack through various flapping rates. For each value of the static mean angle of attack of the airfoil section, the trailing edge flap motion is performed with a fixed airfoil angle amplitudes of 0 and 10 degrees. The objective is to assess the effects of the effective angle of attack caused by the flap deflection on the flow dynamics, and provide data to compare with Leishman's analytical model at different flap reduced frequencies. Results show good agreement with Leishman's model at a lower amplitudes and frequency of oscillations, but larger discrepancies at higher amplitudes and frequency of oscillations were observed.

Nomenclature

b	Airfoil semi-chord ($c/2$)
C_L	Lift coefficients
e	Flap hinge location, semichord
f	Forcing frequency (Hz)
h_a	Plunging displacement (half stroke)
k	Reduced frequency $\pi fc/U_\infty$
ℓ	Wing span (m)
δ	Flap deflection angle
q	non-dimensional pitch rate, $\frac{\dot{\alpha}c}{V}$
Re	Reynolds number
S	distance traveled in semichords, $\frac{2Vt}{c}$
t	Time (s)
U_∞	Free stream velocity
α_0	Airfoil mean angle of attack
α_{eff}	Effective angle of attack
δ_0	Mean flap deflection angle
δ_A	Flap deflection amplitude
ω	Angular frequency,(rad/s)
ρ	Air density
qs	Quasi-steady
AoA	Angle of attack

*PhD student, Engineering Mechanics, BEAM department, Virginia Tech., Blacksburg, VA, 24061, AIAA student member
†Assistant professor, Aerospace Engineering Department, Military Technical College, Cairo, 11766, AIAA Applied Aerodynamic committee member.
‡Professor, Engineering Mechanics, BEAM department, Virginia Tech., Blacksburg, VA, 24061 AIAA member

I. Introduction

Non-conventional lifting mechanisms have been proposed to perform agile missions. Exploiting these mechanisms requires accurate characterization of the unsteady aerodynamics and control laws. The step response and frequency response functions have been proposed and used to model the unsteady aerodynamics over maneuvering airfoils. The work done by Wagner,[1] Prandtl,[2] Theodorsen[3] and Garrick[4] described some fundamental physical concepts in understanding and modeling the unsteady aerodynamics. These concepts are usually incorporated with a potential flow framework and small disturbance theory to obtain analytical expressions of the flow quantities. Unsteady aerodynamics can result from several independent or combined motions such as: pitching,[5–8] plunging[9–14] and surging[15] like birds. Work has been done to explore the associated phenomena related to those motions. Dynamic stall[16,17,18] , leading edge suction[19,20] , leading edge vortex[21,22] and vortex trapping[23,24,25] phenomenon are considered as passive non conventional lift force enhancement mechanisms. Using trailing edge flaps (TEF) can also be used as active devices to improve performance and reduce vibrations noise. Leishman[26] formulated a state space model for computing the unsteady lift on an airfoil due to arbitrary motion of a trailing-edge flap. He showed that, for an incompressible case, the state-space form can be obtained based on Duhamel superposition via employing an improved exponential approximation to Wagner's indicial lift function. A number of passive and active dynamic-stall flow-control concepts, such as the use of a trailing-edge flap can be found from Rennie et al.,[27] Nguyen et al.[28] and Feszty et al.[29] Trailing-edge flaps have been used extensively as a routine method of controlling lift by temporarily altering airfoil camber on an airplane in steady low-speed operations, especially during takeoff and landing, without penalizing cruise performance. More recently, trailing-edge flaps have been used as unsteady aerodynamic control devices for the control of transient lift on maneuvering fighter aircraft and large negative pitch moment on helicopter rotor blades, as well as in an attempt to control unsteady lift, including flutter suppression and gust alleviation. Airfoil lift characteristics for unsteady trailing-edge flap motions were first analyzed by Theodorsen[3] for harmonically oscillating flaps.

Gerontakos and Lee[30] studied the effects of movable TEF on an oscillating NACA-0015 wing. Their experiment was performed at Re = 1.65 x 10^5 and at a reduced frequency of 0.05 while considering upward and downward flap deflection and a mean angle of attack variation of $\alpha_0 = 10°$, 12.5° and 15°. Upward deflection of the flap results in reducing the negative $C_{m,peak}$. Consequently, increasing the flap deflections leads to more efficient reduction mechanism. Their most significant finding is that the leading edge vortex (LEV) formation and detachment were not affected by the TEF motion, whereas the low-pressure signature of the LEV was reduced by the upward flap deflection. They extended their work by performing particle image velocimetry (PIV) measurements on the same profile.[31] The authors asserted that the initiation, growth and detachment of the LEV were largely unaffected. In addition, for an upward flap deflection, no trailing edge Vortex (TEV) was observed and for the downward TEF deflection did not render any significant change in the formation and detachment of the LEV.

In this work, we investigate experimentally an actuated flapped airfoil at two mean angles of attack; 0° and 10°. The effects of a movable trailing-edge flap for a NACA-0012 airfoil pitching rate, actuation start time, and flap deflection angles on the critical aerodynamic values were measured. Experiments were conducted in an open circuit wind tunnel considering two cases, a) Static measurements for both airfoil and deflected flap positions , b) Dynamic measurements for airfoil with various trailing edge flap rates. Our interest is in the assessment of the effects of the actuated trailing flaps with different mean angle of attack and the synchronization of the flap on lift through comparison with Leishman's model.

II. Flow Facility and Force Measurement Instrumentation

A. The Flow facility

The experiments were performed in the subsonic wind tunnel facility at Virginia Tech shown in fig.1. The tunnel is a suction-type open circuit wind tunnel powered by a 15 hp Leeson motor driving a 1 meter centrifugal fan. The air flow is discharged by the fan which forces the flow to pass through a square (1.5 m × 1.5 m) honeycomb inlet that has a cell size of 0.09 m by 0.001 m cell size. This inlet is followed by three turbulence reduction screens that ensure a uniform flow with acceptable turbulence intensity of less than 0.2% at 10 m/s. The test chamber dimension is 120 cm × 52 cm × 52 cm. The wing model was mounted horizontally at the center of the wind tunnel test section. The origin of the coordinates was located at the leading edge of the airfoil with x, y and z in the streamwise, transverse and spanwise direction,

respectively. The wing model extends the whole test section width and a gap between the wing tips and the tunnel walls was kept at less than 1 mm to minimize the leakage flow through the gap. A long time series pressure measurements via pitot static tube was taken spanwise the test section using traverse system. The non-uniformity was found to be 3% of the free stream velocity. The air speed is measured using a pitot tube via a scanni-valve pressure transducer that provides readings with an accuracy of 0.5% of the flow velocity.

Figure 1. The tested wing fixed in the wind tunnel

B. Pitch-Flapped Mechanism

The wing was fabricated from a foam core with a NACA 0012 profile, reinforced with a solid rod of carbon fiber of diameter 4 mm at quarter chord location spanwise and two layers of carbon fabric ($60gm/cm^2$) finished with two layers of epoxy paste. The wing chord length is $c = 7\,cm$, maximum thickness to chord ratio is $t/c = 0.12$%c and the model spans the entire width of the wind tunnel test section of length $0.52\,m$. The wing was also equipped with a plain full-span 25%c trailing-edge flap (hinged at 0.75%c), which can be deflected harmonically both in-phase and 180^o out-of-phase, relative to the airfoil motion ,with a maximum deflection amplitude δ_{max} of 30^o. The wing is pivoted via hinge at the quarter chord location with a main fixed rod of 1.5 cm in diameter attached to the load cell. A fairing bracket holding 2 digital servo motors is fixed on the lower half of the rod responsible for the oscillatory motion of the airfoil and the trailing edge flaps. Each servo motor is connected to the surface via steel push rod of diameter 1.5 mm and controlled using a micro Maestro 6-Channel USB Servo Controller connected to a computer. At mid chord location the flap has a carbon fiber strip with equidistant holes (2 mm) to achieve higher deflections with the controller. The instantaneous angle of attack of the airfoil was fed to the controller with an error of 0.2^o. The schematic diagram of the setup fixation is shown in fig.2.

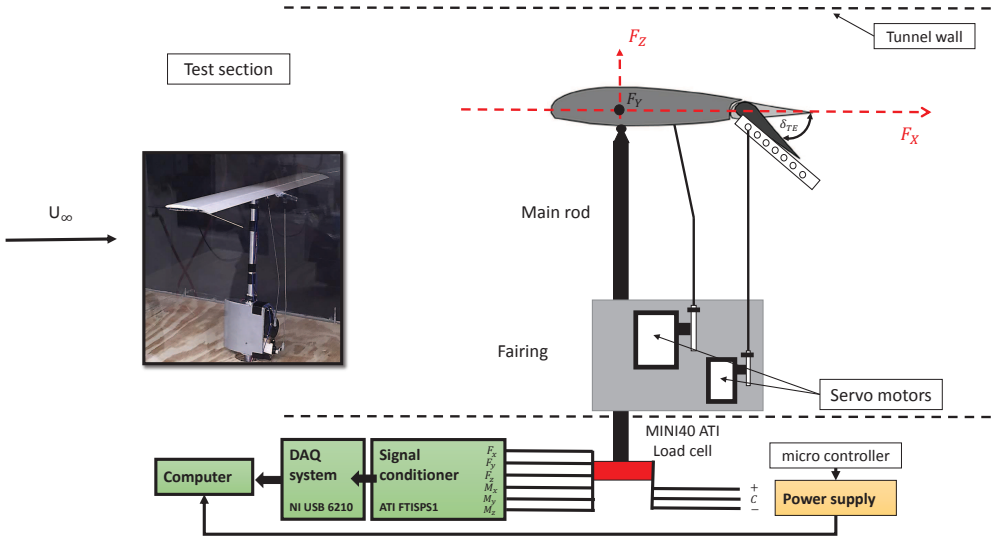

Figure 2. Schematic for the tested mechanism fixed inside the tunnel

The whole setup (wing and load cell) was connected to a fixed bracket below the test section attached to a strut mount. The bracket have one degree of freedom to move in vertical direction using a stepper motor controlled by VELEMX 8300 external controller. The setup has a structurally stiff arrangement suitable for very aggressive motions. The angle fed form the controller to the flap was verified using three-axis gyro fixed at mid the flap chord and connected to Arduino UNO board. A digital protractor was used to measure the angle of the wing before and after motion and verified from the controller signal with an error of $\pm 0.2^o$.

C. Force measurements

The direct force measurements consists of a force/torque sensor (ATI Industrial Automation Mini40 force/torque sensor), interface power supply (ATI industrial Automation 9105-IFPS-1), a data acquisition card (National Instruments PCI-662) and a computer. The wing model and the main rod was attached to the metric side of the sensor using a circular bracket. The fixed side of the sensor is attached to a fixed strut right angle plate as shown in Fig.3. The Mini40 sensor is a six-component silicon strain gauge sensor capable of measuring forces in the plane of the airfoil cross-section up to ± 80 N and ± 240 N in the orthogonal direction. It also measures torque up to ± 4 N.m in all three axes. The force resolution is 1/50 N (F_x and F_y) and 1/25 (F_z) for force and 1/2000 N.m for torque. The force sensor measures force normal to the model, F_z, along the span, F_y, and along the model's longitudinal axis, F_x. Force data processing is performed in the sensor frame of reference.

Two different experiments were performed to obtain the force time history: a tare experiment and a force experiment. The tare experiments were performed with wind-on to measure the tare load on the force/torque sensor before attaching the main rod to the wing model without changing any other experimental parameter. The generated loads from the main rod holding the wing profile and the fairing of the servo motors were subtracted from the force measurements of the whole setup with the wing attached to obtain the applied aerodynamic loading.

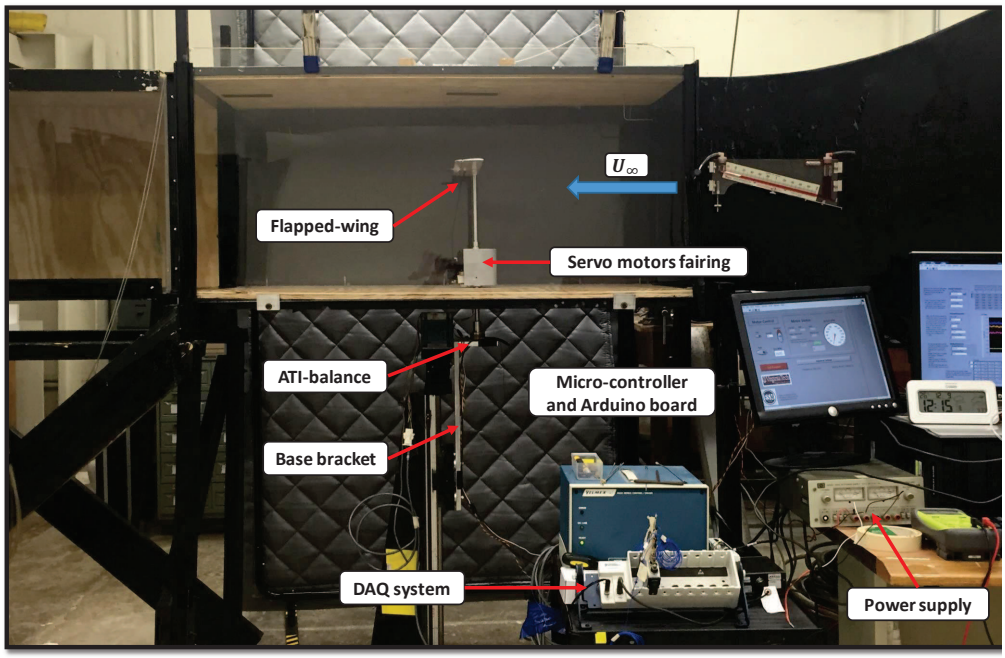

Figure 3. The used devices in the experimental testing

The data was collected and processed using National Instruments Nidaq-9172 and Nidaq USB-6210 with sampling frequency rate of 1000 Hz. The data was smoothed using digital fourth-order butterworth low pass filter. A typical power spectrum before and after applying filter was done within all the unsteady runs. All force measurements were based on an ensemble of 100 clean cycles, sampled at 1 kHz with 10 seconds of pre-trigger data, where the first ten cycles as well as the last ten cycles were cut away due to aerodynamic and inertial starting and stopping effects. To subtract the dynamic tare for a given case, a corresponding ensemble of 100 clean cycles was measured with the wind tunnel turned off. Therefore, in this work, dynamic tare was done before and after data recording in wind off mode processing with the data obtained from the flap motion.

The primary source of uncertainty for the clean wing is the angle of attack setting, accurate to within 0.2°. The overall error in force coefficient measurements was found to be 3% accounting for errors in flow speed, angle of attack, bias error introduced during calibration, and sampling precision. Errors associated with the installation of trailing edge length and deployment the prescribed angle. Due to these variations, the force coefficient for these configurations have an uncertainty closer to 4%. Wind tunnel boundary corrections were calculated using the methods of Pope and Harper.[32] Calculations of the solid two-dimensional blockage factor, wake blockage, and correction for streamline curvature. Eventually, these effects lead to uncertainty in lift coefficient measurements of $\pm$ 0.012 C_L. The effects of the length of the bar connecting the servo to flap hinge point results in a time constant delay on force measurements at operating frequencies above 2.5 Hz. For this reason, k=0.12 is the limit on reduced frequency for these test conditions.

D. Problem formulation

The unsteady lift on an airfoil with a harmonically oscillating flap in incompressible flow has been studied by Kiissner and Schwarz,[33] but the most well known solution is that of Theodorsen's.[34] The lift on a thin rigid airfoil undergoing oscillatory forcing (Fig.4) can be written in coefficient form as:

$$C_L = \frac{\pi b}{U_\infty^2}\left(\ddot{h} + U_\infty \dot{\alpha} - ba\ddot{\alpha}\right) + 2\pi C(k)\left(\frac{\dot{h}}{U_\infty} + \alpha + b\left(\frac{1}{2} - a\right)\frac{\dot{\alpha}}{U_\infty}\right) \quad (1)$$

In another format, the lift force (L) per unit span is,

$$L = \underbrace{\pi\rho b^2\Big(\ddot{h} + U_\infty\dot{\alpha} - ba\ddot{\alpha}\Big)}_{Added\ mass} + \underbrace{2\pi\rho U_\infty b\Big(\dot{h} + U_\infty\alpha + b(\frac{1}{2} - a)\dot{\alpha}\Big)}_{Quasi\ steady} C(k) \tag{2}$$

where, $\ddot{h}$ and $\ddot{\alpha}$ are plunging and pitching accelerations respectively.

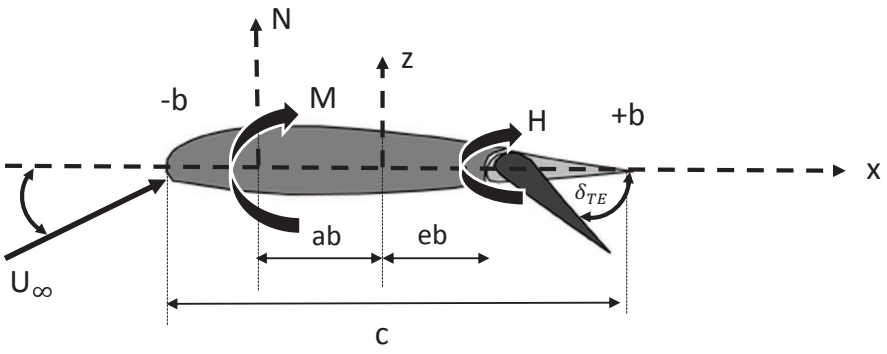

Figure 4. Nomenclature of airfoil with trailing edge flap

The first group of terms are the non-circulatory components that account for the inertia of the fluid. The second group of terms are the circulatory components, where $C(k)$ accounts for the influence of the shed wake vorticity (lift deficiency factor). With the addition of a trailing-edge flap with hinge at a distance eb from the mid-chord, there are additional air loads that depend on δ_{TE} and its time rate-of-change $\dot{\delta_{TE}}$. The total lift is expressed as:

$$C_L(t) = \frac{\pi b}{U_\infty^2}\big(\ddot{h} + U_\infty\dot{\alpha} - ba\ddot{\alpha}\big) + \frac{b}{U_\infty^2}\big(-U_\infty F_4\dot{\delta} - bF_1\ddot{\delta}\big) + 2\pi C(k)\big(\alpha_{qs} + \delta_{qs}\big) \tag{3}$$

where F_1, F_4, F_{10} and F_{11} are geometric terms that depend only on the size of the flap relative to the airfoil chord. α_{qs} is the quasi-steady airfoil angle of attack, and δ_{qs} is the quasi-steady angle of attack due to the imposed flap deflection. For a coordinate system located at mid-chord, the geometric terms can be expressed as:

$$F_1 = e\,cos^{-1}\,e - \frac{1}{3}(2 + e^2)\sqrt{1 - e^2} \tag{4}$$

$$F_4 = e\,\sqrt{1 - e^2} - cos^{-1}\,e \tag{5}$$

$$F_{10} = \sqrt{1 - e^2} - cos^{-1}\,e \tag{6}$$

$$F_{11} = (1 - 2e)\,cos^{-1}\,e + (2 - e)\sqrt{1 - e^2} \tag{7}$$

and the quasi-steady lift due to airfoil angle of attach and due to flap deflection is written as:

$$\alpha_{qs} = \left[\frac{\dot{h}}{U_\infty} + \alpha + b(\frac{1}{2} - a)\frac{\dot{\alpha}}{U_\infty}\right] \tag{8}$$

$$\delta_{qs} = \left[\frac{F_{10}\delta}{\pi} + \frac{F_{11}\dot{\delta}c}{4\pi U_\infty}\right] \tag{9}$$

For the case of arbitrary airfoil motion and/or arbitrary flap deflection, the result for the unsteady lift can be obtained by means of Duhamel's superposition integral with the Wagner indicial (step) response, and is written as:

$$C_L(t) = \frac{\pi b}{U_\infty^2}\left(\ddot{h} + U_\infty\dot{\alpha} - ba\ddot{\alpha}\right) + \frac{b}{U_\infty^2}\left(-U_\infty F_4\dot{\delta} - bF_1\ddot{\delta}\right) + 2\pi\Big(\alpha_{qs}(0)\phi_w(S) + \int_0^S \frac{d\alpha_{qs}}{d\sigma}\phi_w(S-\sigma)d\sigma + \delta_{qs}\phi_w(S) + \int_0^S \frac{d\delta_{qs}}{d\sigma}\phi_w(S-\sigma)d\sigma\Big) \quad (10)$$

Therefore, the total lift due to independent arbitrary airfoil motion and flap deflection is written as:

$$C_L^c(t) = C_{L\alpha}^c(t) + C_{L\delta}^c(t) + C_L^{Nc}(t) \quad (11)$$

Building the state space model for the given problem, the same formulation given by Leishman[26] can be used to calculate the amplitude due to circulatory lift $(A_c) = C_{L\,circ} - \overline{C_{L\,circ}}$.

III. Experimental measurements

The aim is to deduce the effect of a clean configuration for a static airfoil with and without flap deflection in a static and dynamic modes. The experimental constraints are designed to give a broad measurement range from linear to stall regime. The experiments is conducted at a low operating Reynolds number of 21,000. The flap deflection static measurements were done for flap angles of positive 5^o, 8^o and 10^o degrees, while the dynamic modes of operation were done for flap deflection angles of ($\pm 5^o$, $\pm 8^o$ and $\pm 10^o$) operating at frequencies tabulated in Table 1.

Table 1. Experiment dynamic operating conditions

Mean Angle of Attack α_0 (Deg)	Flap Deflection (Deg)	Reduced frequency (k)
0^o,10^o fixed	± 5,± 8, ± 10	0.023 - 0.12

The simple harmonic flap oscillation is prescribed as $\delta = \delta_0 + \delta_A Sin(\omega t)$. The forcing frequency f comes from $\omega = 2\pi f$, δ_0 is the mean flap position while δ_A is the flap amplitude.

A linear relation between the excitation and the unsteady aerodynamic response is assumed to be harmonic. This is valid for thin airfoil theory, or airfoils that deflect at small amplitudes of oscillation. But the presence of flow separation is the result of unsteady aerodynamic response. The aerodynamic response also has a nonlinear relationship with flap deflection.

IV. Results and Discussions

A. Quasi-steady lift measurements

The steady lift measurements were performed for a broad range of angles of attack to obtain the quasi-steady lift calculation based on the static curve for clean configuration followed by the flap deflection static lift. The static flap deflection configurations are listed in Table 2.

Table 2. Experiment operating conditions and constraints

Name	Range
Reynolds No. (Re)	21,000
Mean angle of attack (α_0)	0^o - 28^o
Flapped Deflection. (δ)	5^o, 8^o, 10^o, 15^o

Figure 5 (a) shows the measured experimental static lift curves are in agreement with the data published by Laitone[35] and Alam.[36] The static lift curve slopes is far from the conventional $2\pi\alpha$ that is expected for higher Reynolds number. Figure 5 (b) shows the experimental quasi steady lift curve results along with static flap deflections at Reynolds number of 21,000.

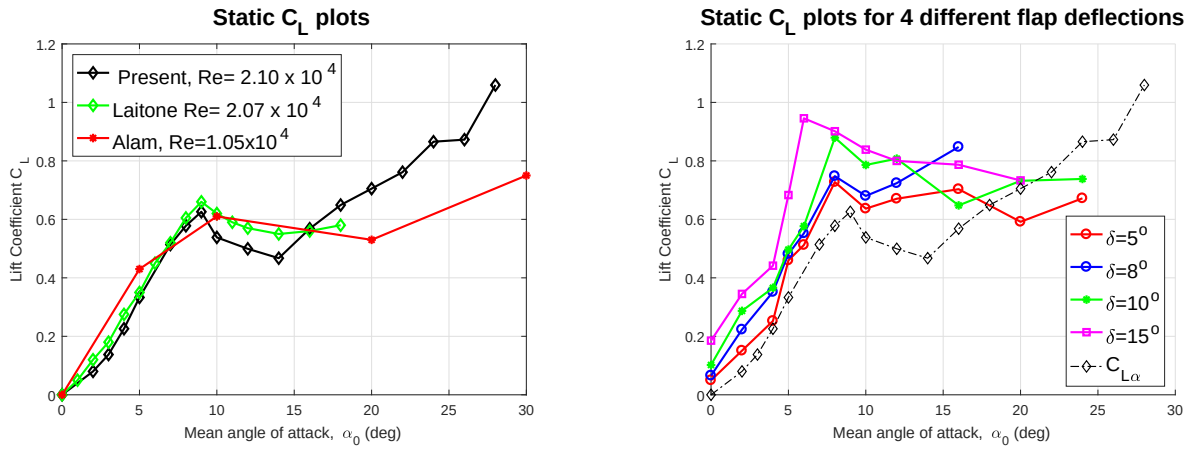

(a) Static lift curve at Re = 21,000

(b) Static lift curve for different flap settings at Re = 21,000

Figure 5. Plain and flapped static measurements for NACA-0012 airfoil

Figure 6 shows the quasi-steady measurements at α_0 of 0^o and 10^o by only varying the flap angle δ downwards. Both test cases were repeated three times to obtain the averaged results. The values of lift coefficient at flap angle of 0 degrees for α_0 of 0^o and 10^o are introduced into the quasi-steady term of Leishman's semi empirical formulation to match the initial parameters of the flow regime being experimented on. The corresponding quasi-steady values of $C_L = 2\pi(\alpha_{qs} + \delta_{qs})$ used for 0^o and 10^o at $\delta_0 = 0^o$ mean flap angle were 0.005 and 0.513 respectively.

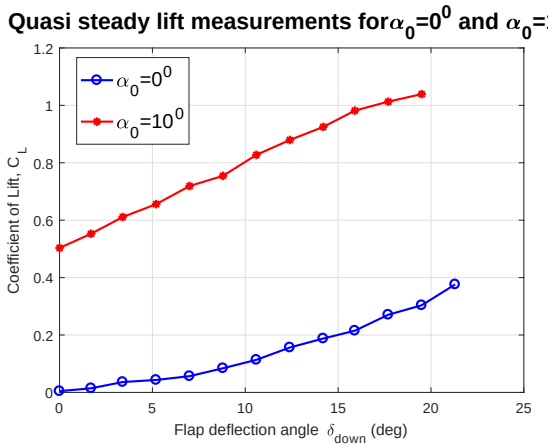

Figure 6. Quasi lift measurements for various flap deflections at mean angles of attack 0 deg and 10 deg

B. Dynamic measurements

The dynamic measurements were performed for the configurations listed in Table 1. There is an infinite number of configuration for the flap setting angles that comes along with airfoil angle settings, but the test matrix was set based on the lift curve results, where the range captures the transition between the linear and stall regimes. It is also worthy to select a combination of flap deflections with respect to the airfoil's mean angle of attack close to the boundaries of the operating range for the known fluid flow regimes that can support UAV and MAV applications. The flap deflection rates were varied over a broad range of operating frequencies from 0.5 Hz to 2.5 Hz, which corresponds to reduced frequencies of k= 0.023 to 0.12.

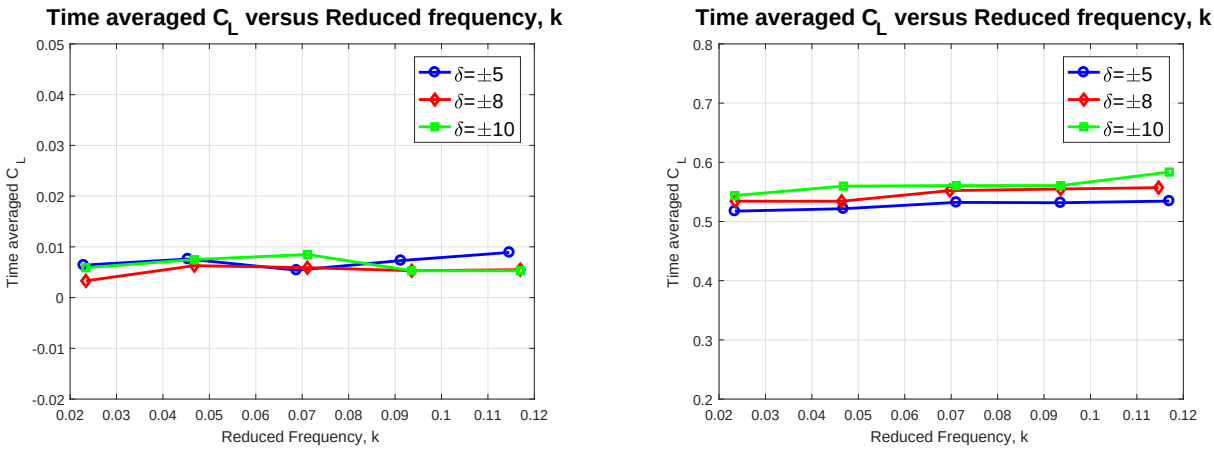

(a) Time averaged C_L for mean angle of attack of 0 deg

(b) Time averaged C_L for mean angle of attack of 10 deg

Figure 7. Dynamic measurements for NACA-0012 airfoil at different flap settings

Time averaged lift coefficients as a result of harmonic flap motion were collected in two separate plots as shown in 7 for various reduced flap frequencies. The airfoil's AoA was fixed at $\alpha_0 = 0^o$ and at 10^o. The lift coefficient gathered from the time averaged dynamics was computed over 8 seconds of real time data.

The static C_L value at $\alpha_0 = 0^o$ and $\delta_0 = 0^o$ is 0.005. Figure 7 (a) shows the mean C_L for $\delta_A = \pm 5^o$, $\pm 8^o$ and $\pm 10^o$. Despite the fact that flap oscillations moves from quasi steady to unsteady flow regime ($k > 0.05$), the flow remains fully attached and almost symmetric in pitch up and pitch down motions. The time averaged lift from dynamic measurements is expected to remain close to this value as the flap angles change with increasing oscillating frequency.

We observed slightly improved values for time averaged lift at $\alpha_0 = 10^o$ relative to it's static value. The static C_L value for this setting at $\delta_0 = 0^o$ is 0.513. The fact that time average lifts are different from their corresponding static values also raises questions about the symmetry of aerodynamic behavior during the upstroke and down-stroke motions. The flap experiences different flow behaviors at these two motions, which leads us to further investigate the hysteresis effects of this dynamic. The operating Reynolds number plays a vital role in this condition too since it is operating in a laminar-transition regime.

In general, no significant differences between the dynamic and static values for this set of data were observed at smaller amplitudes and frequencies, but we observe a small step change in time averaged lift for all three flap settings at ($k > 0.05$) for mean angle of attack of 10 deg. Beyond this point, a considerable increase in mean C_L averaged value was noticed for $\delta_A = \pm 8$ and ± 10, where the presence of onset flow separation plays a role in the shift of the time averaged lift away from their corresponding static C_L values.

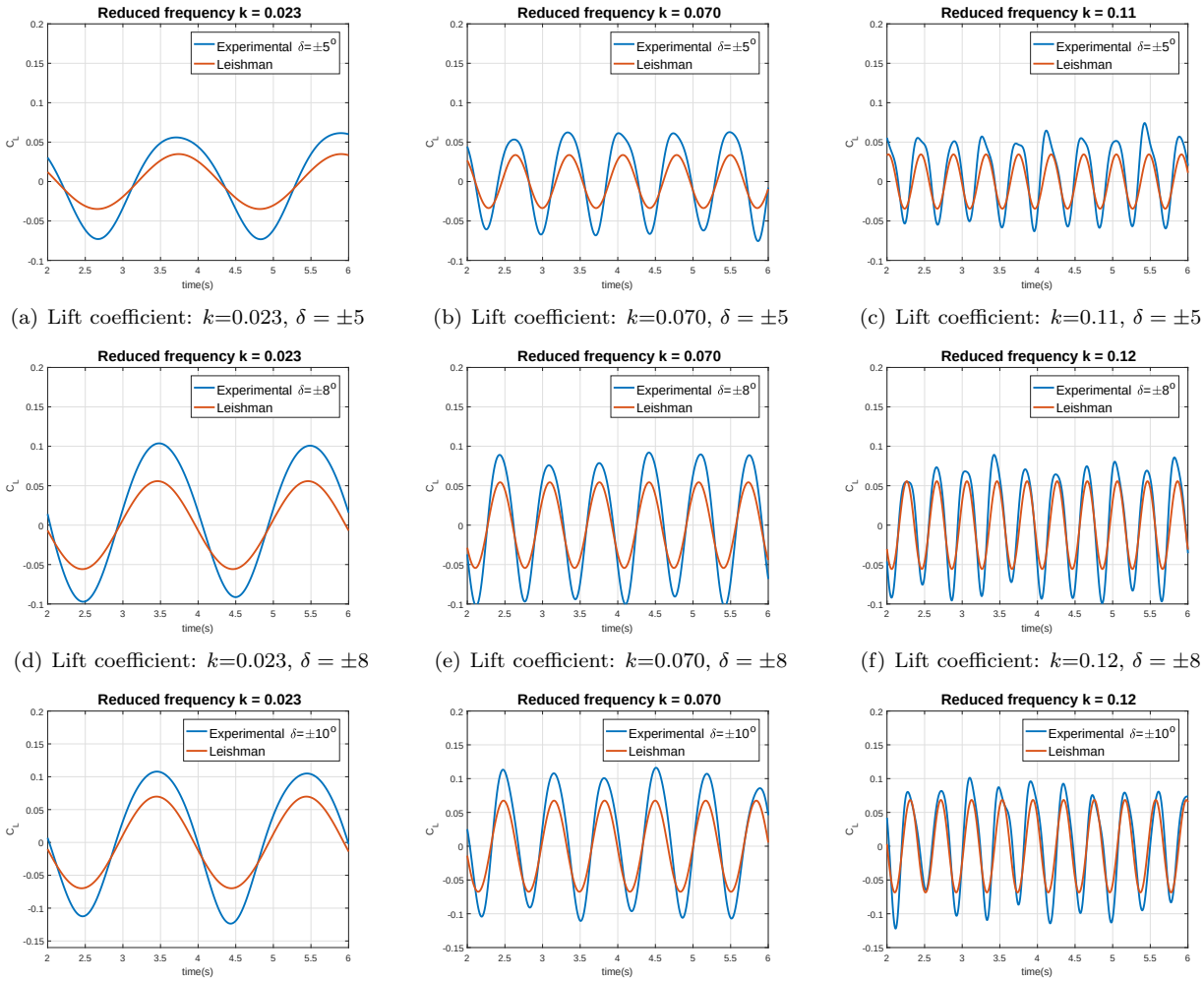

(a) Lift coefficient: k=0.023, $\delta = \pm 5$ (b) Lift coefficient: k=0.070, $\delta = \pm 5$ (c) Lift coefficient: k=0.11, $\delta = \pm 5$

(d) Lift coefficient: k=0.023, $\delta = \pm 8$ (e) Lift coefficient: k=0.070, $\delta = \pm 8$ (f) Lift coefficient: k=0.12, $\delta = \pm 8$

(g) Lift coefficient: k=0.023, $\delta = \pm 10$ (h) Lift coefficient: k=0.070, $\delta = \pm 10$ (i) Lift coefficient: k=0.12, $\delta = \pm 10$

Figure 8. Time history lift coefficients for experimental data versus Leishman's indicial formulation at $\alpha_0 = 0^o$

Figure 8 shows the time history of C_L over a steady state period of data for δ_A=$\pm 5^o$, $\pm 8^o$ and $\pm 10^o$ degrees at mean angle of attack $\alpha_0 = 0^o$. The dynamic characteristics responds with excellent agreement to Leishman's formulation. We note that at a reduced frequency of 0.12, the upstroke and downstroke motions of the flap from the experimental data begins to lose some symmetry. For reduced frequencies of 0.023 and 0.070, the regime of flow can be characterized as quasi-steady and transition from quasi-steady to unsteady respectively. At these reduced frequencies, most of the time series' symmetry is retained during the upstroke and downstroke motions of the flap, with only minor under predictions demonstrated by Leishman's model compared to the experimental results.

At these fully attached flow conditions, the flap experiences enhanced instantaneous peak lifts when it is in motion than when it is steady for reduced frequencies of k=0.023 and k=0.07. For the dynamic case at k=0.12 with deflections of δ_A=$\pm 10^o$, the flap experiences a drop in maximum instantaneous lift, resulting in lower values than its static value for the same flap deflection angle. This is expected as the effects of wake due to vortex shedding plays a bigger role in lift deficiency at higher reduced frequencies. The effective angle of attack for flap deflections $\delta_A = +5^o$, $+8^o$ and $+10^o$ degrees are approximately $\alpha_{eff} = 1.36^o$, 2.17^o and 2.72^o respectively.

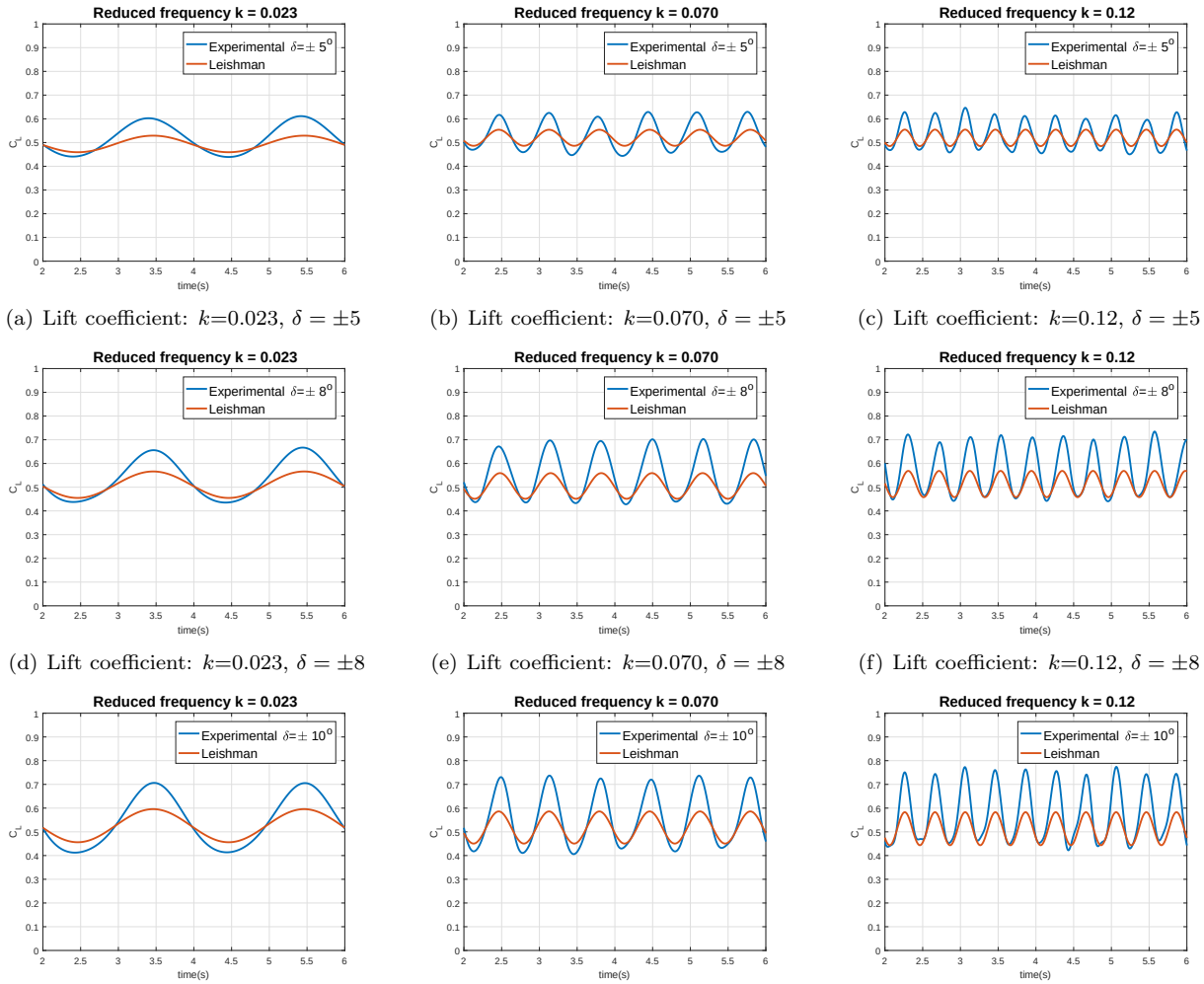

(a) Lift coefficient: k=0.023, $\delta = \pm 5$ (b) Lift coefficient: k=0.070, $\delta = \pm 5$ (c) Lift coefficient: k=0.12, $\delta = \pm 5$

(d) Lift coefficient: k=0.023, $\delta = \pm 8$ (e) Lift coefficient: k=0.070, $\delta = \pm 8$ (f) Lift coefficient: k=0.12, $\delta = \pm 8$

(g) Lift coefficient: k=0.023, $\delta = \pm 10$ (h) Lift coefficient: k=0.070, $\delta = \pm 10$ (i) Lift coefficient: k=0.12, $\delta = \pm 10$

Figure 9. Time history lift coefficients for experimental data versus Leishman's indicial formulation at $\alpha_0 = 10^o$

Figure 9 shows the time history of C_L over a steady state period of data in comparison with Leishman's formulation at fixed mean angle of attack of $\alpha_0 = 10^o$. At this stall condition of the airfoil, there is no enhanced lift for the dynamics case compared to its static counterpart. The effective angle of attack for flap deflections δ_A of +5 degrees, +8 degrees and +10 degrees are approximately $\alpha_{eff} = 11.43^o$, 12.26^o and 12.82^o respectively. So for a full flap deflection motion, the airfoil alternates around the stall angle of attack. Further to this, larger discrepancies from Leishman's model were observed at higher flap deflection angles and reduced frequencies. It is interesting to note that at lower frequencies, experimental data agrees very well with Leishman's model. However, at larger angles of flap deflection combined with high unsteady motion at reduced frequencies of 0.07 and 0.12, flow separation becomes more apparent. As a result, there is no match between Leishman's model and the experimental measurements at these flap settings. The asymmetric aerodynamic behavior at higher frequencies also causes some shift effect of the mean C_L at deflection angles of $\pm 8^o$ and $\pm 10^o$.

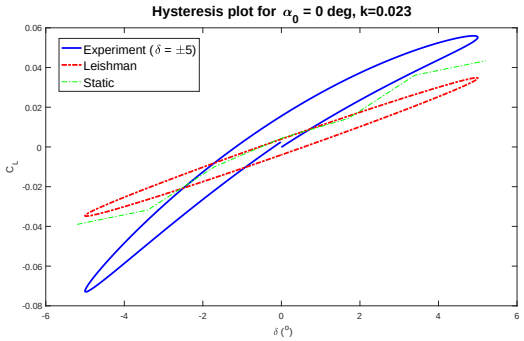

(a) Lift coefficient versus $\delta = \pm 5^o$, k =0.023

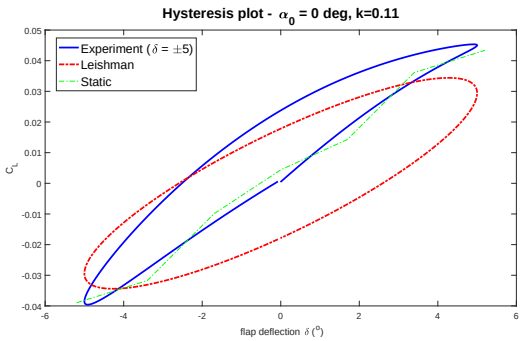

(b) Lift coefficient versus $\delta = \pm 5^o$, k =0.11

Figure 10. Hysteresis plots for $\delta \pm 5^o$ at $\alpha_0 = 0^o$

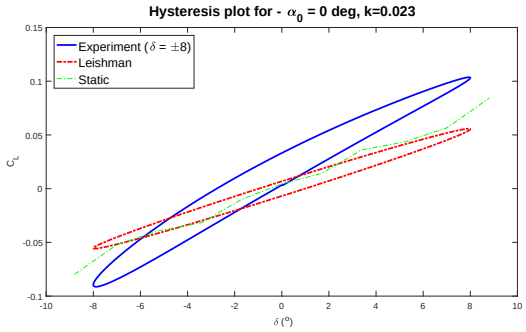

(a) Lift coefficient versus $\delta \pm 8^o$, k =0.023

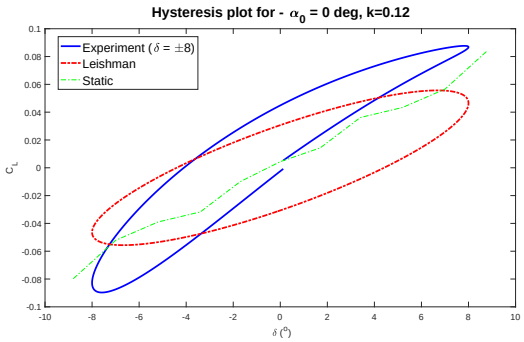

(b) Lift coefficient versus $\delta \pm 8^o$, k =0.12

Figure 11. Hysteresis plots for $\delta \pm 8^o$ at $\alpha_0 = 0^o$

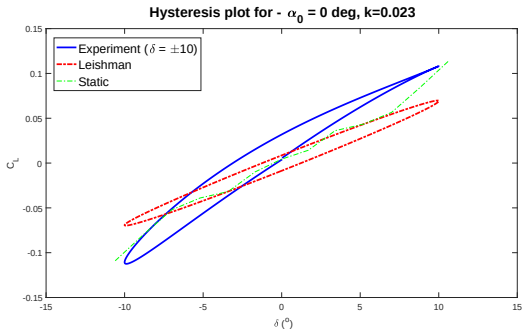

(a) Lift coefficient versus $\delta \pm 10^o$, k =0.023

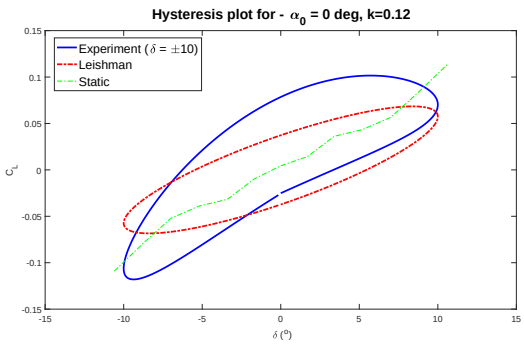

(b) Lift coefficient versus $\delta \pm 10^o$, k =0.12

Figure 12. Hysteresis plots for $\delta \pm 10^o$ at $\alpha_0 = 0^o$

Figures 10, 11 and 12 show the instantaneous lift near the flap in upstroke and downstroke motion respectively while mean angle of attack is fixed at $\alpha_0 = 0^o$. The left column represents flap oscillations at reduced frequency k=0.023, and the right column represents the flap oscillations with the same amplitude conditions but for k=0.12. Hysteresis loops were plotted using a period where steady state condition is dominant as visualized by a fully closed loop. The small gap of the hysteresis loop at low amplitudes of oscillations indicate that the flow is fully attached like what Leishman predicts. The widening of the gaps for the same flap settings were observed for higher reduced frequencies and for flap deflection amplitudes of 8 and 10 degrees. The hysteresis effects are significant when the flow begins to separate from a fully attached flow as a result of high angles of attack. The unsteady response is captured by the experimental program

that isn't caught by Leishman's model. An experimental static curve line is also added to compare with the effects of the lift due to dynamic oscillations. It's clear that the dynamic case for this airfoil setting produces larger maximum lift than its corresponding static lift when the flap is at a maximum downward deflection. However, this claim is does not hold for $\alpha_0 = 10^0$ oscillating at k=0.12.

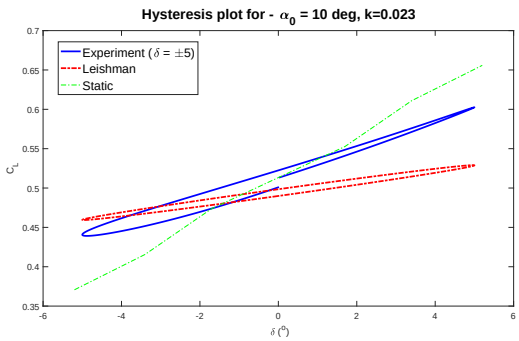

(a) Lift coefficient versus $\delta = \pm 5^o$, k =0.023

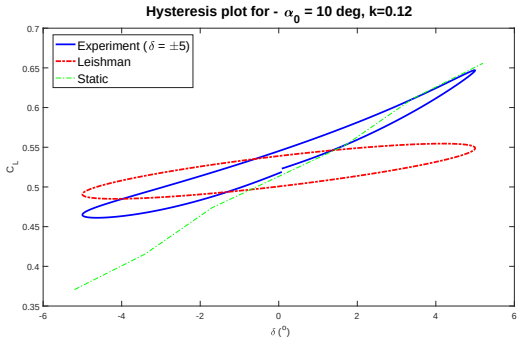

(b) Lift coefficient versus $\delta = \pm 5^o$, k =0.12

Figure 13. Hysteresis plots for $\delta \pm 5^o$ at $\alpha_0 = 10^o$

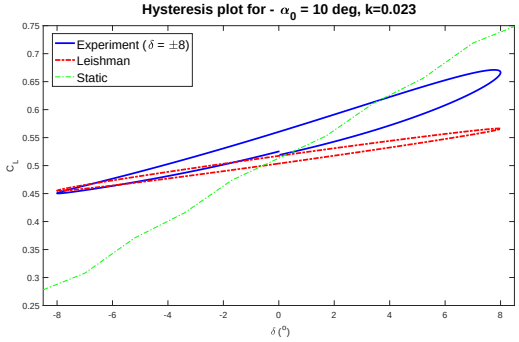

(a) Lift coefficient versus $\delta \pm 8^o$, k =0.023

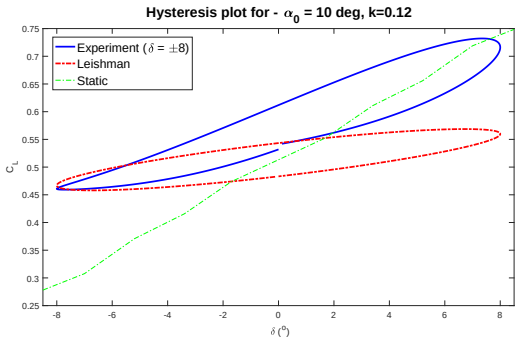

(b) Lift coefficient versus $\delta \pm 8^o$, k =0.12

Figure 14. Hysteresis plots for $\delta \pm 8^o$ at $\alpha_0 = 10^o$

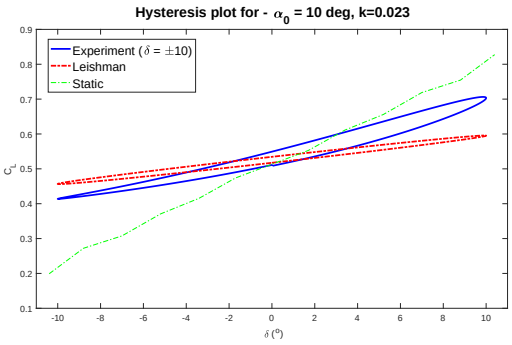

(a) Lift coefficient versus $\delta \pm 10^o$, k =0.023

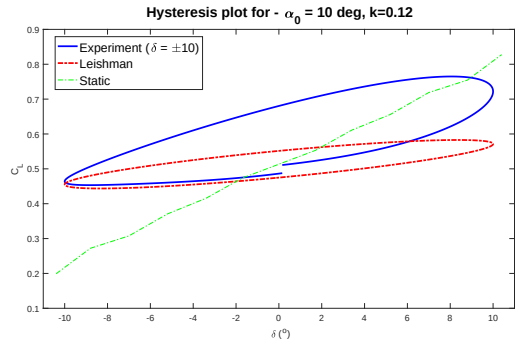

(b) Lift coefficient versus $\delta \pm 10^o$, k =0.12

Figure 15. Hysteresis plots for $\delta \pm 10^o$ at $\alpha_0 = 10^o$

Figures 13, 14, 15 show the instantaneous lift near the flap in upstroke and downstroke motion respectively while the mean angle of attack is fixed at $\alpha_0 = 10^o$. An upstroke phase and at a low angles of flap deflections suggest that the flow is mostly attached to the surface. At larger deflection angles of 8 and 10 degrees, the gap widening occurs as a result of possible flow separation . Also, the direction of the hysteresis loops are all

consistent with a counter-clockwise motion. The slope of the experimental hysteresis loop increases compared to the slope of the static lift curve and the slope of Leishman's hysteresis loop. This change in slope may be attributed to the contribution of the circulatory lift and the added mass effects while increasing the mean AOA and the operating frequency, which results in increasing the phase shift between the contributions of the evolved forces. This deviation alleviates as the oscillating frequency increases as a result of increased vortex shedding.

V. Conclusion

The objective of this work is to asses lift alleviations that may occur at specific reduced frequencies, and that could possibly produce a new non-conventional lifting mechanism. The TEF results show that:

(i) Time averaged lift coefficient remains almost the same compared to its quasi-steady for small oscillations. Differences are apparent at flap deflection angles of 8 and 10 degrees oscillating at reduced frequencies above k=0.05.

(ii) A total instantaneous lift alleviation was observed for the dynamics case for all flap deflections at mean angle of attack of α_0= 0 degrees except at $\delta_A = \pm 10^o$ and at a reduced frequency of k=0.12. Predictions made by Leishman's model here agrees very well with the experimental measurements.

(iii) For the dynamic case at $\alpha_0 = 10^o$, total instantaneous lift alleviation was only observed for flap deflections of δ_A=$\pm 5^o$ and $\pm 8^o$, but no lift enhancement relative to the static lift was observed at all the operating frequencies for flap deflection $\delta_A = \pm 10^o$. Predictions by Leishman's model for this case do not match with the experimental measurements.

(iv) Hysteresis plots show that the gap of the loop and the slope of the loop changes significantly with increasing reduced frequencies. The gap widening is pronounced at higher angles of attack and higher reduced frequency where the possibility of flow separation is evident. The contribution of circulation due to vortex shedding and added mass plays a significant role in phase shifts between the evolved forces that are not caught by Leishman's semi-empirical model.

Experimental results for hysteresis show a deviation in the slope, with an increase in the hysteresis minor axis compared to Lieshman's model. The reason is because the used model is based on a state space representation (linear model) up to a limit of flow regime, and does not account for the full physics such as leading edge vortex and dynamic stall that may occur beyond that limit. These observations may be verified using particle image velocimetry measurements or dye injections as flow visualization techniques.

References

[1]Wagner, H., "Uber die Entstehung des dynamischen Auftriebes von Traflgugeln," *Zeitschrift fur Angewandte Mathematic und Mechanik*, Vol. 35, 1925, pp. 17.

[2]Tietjens, O. K. G. and Prandtl, L., *Applied hydro-and aeromechanics: based on lectures of L. Prandtl*, Courier Dover Publications, 1957.

[3]Theodorsen, T. and Mutchler, W., "General theory of aerodynamic instability and the mechanism of flutter," 1935.

[4]Garrick, I. E., "On some reciprocal relations in the theory of nonstationary flows," Tech. Rep. 629, NACA, 1938.

[5]Pruski, B. J. and Bowersox, R., "Leading-Edge Flow Structure of a Dynamically Pitching NACA 0012 Airfoil," *AIAA journal*, Vol. 51, No. 5, 2013, pp. 1042–1053.

[6]Ramesh, K., Gopalarathnam, A., Edwards, J. R., Ol, M. V., and Granlund, K., "An unsteady airfoil theory applied to pitching motions validated against experiment and computation." *Theoretical and Computational Fluid Dynamics*, 2013, pp. 1–22.

[7]Rival, D. and Tropea, C., "Characteristics of pitching and plunging airfoils under dynamic-stall conditions," *Journal of Aircraft*, Vol. 47, No. 1, 2010, pp. 80–86.

[8]Michael, V., "Motion Kinematics vs. Angle of Attack Effects in High-Frequency Airfoil Pitch/Plunge," *Proceedings of 38th Fluid Dynamics Conference and Exhibit 23 - 26 June 2008, Seattle, Washington — AIAA 2008-3822*.

[9]Cleaver, D. J., Wang, Z., and Gursul, I., "Bifurcating flows of plunging aerofoils at high Strouhal numbers," *Journal of Fluid Mechanics*, Vol. 708, 2012, pp. 349–376.

[10]Buchholz, J. H., Panah, A. E., Akkala, J. M., Wabick, K. J., and Wojcik, C. J., "Vorticity Generation and Transport on a Plunging Wing," 2014.

[11]Panah, A. E. and Buchholz, J. H., "Parameter dependence of vortex interactions on a two-dimensional plunging plate," *Experiments in Fluids*, Vol. 55, No. 3, 2014, pp. 1–19.

[12]Zakaria, M., Taha, H., and Hajj, M., "Measurement and modeling of lift enhancement on plunging airfoils: A frequency response approach," *Journal of Fluids and Structures*, Vol. 69, 2017, pp. 187–208.

[13]Zakaria, M. Y., Taha, H. E., Hajj, M. R., and Hussein, A. A., "Experimental-Based Unified Unsteady Nonlinear Aerodynamic Modeling For Two-Dimensional Airfoils," *33rd AIAA Applied Aerodynamics Conference*, 2015, p. 3167.

[14]Zakaria, M. Y., Taha, H. E., and Hajj, M. R., "Experimental Investigations of the Lift Frequency Response at High Angles of Attack," *53rd AIAA Aerospace Sciences Meeting*, 2015, p. 1503.

[15]Baik, Y. S., Rausch, J., Bernal, L. P., Shyy, W., and Ol, M. V., "Experimental Study of governing parameters in pitching and plunging airfoil at low Reynolds number," *48th AIAA aerospace sciences meeting including the new horizons forum and aerospace exposition*, 2010, pp. 2010–388.

[16]McAlister, K. W., Carr, L. W., and McCroskey, W. J., "Dynamic stall experiments on the NACA 0012 airfoil," 1978.

[17]McCroskey, W., "The phenomenon of dynamic stall." Tech. rep., DTIC Document, 1981.

[18]Leishman, J. and Beddoes, T., "A Semi-Empirical Model for Dynamic Stall," *Journal of the American Helicopter society*, Vol. 34, No. 3, 1989, pp. 3–17.

[19]Polhamus, E. C., *A concept of the vortex lift of sharp-edge delta wings based on a leading-edge-suction analogy*, National Aeronautics and Space Administration, 1966.

[20]Lamar, J. E., "Extension of leading-edge-suction analogy to wings with separated flow around the side edges at subsonic speeds," 1974.

[21]Ellington, C. P., Van Den Berg, C., Willmott, A. P., and Thomas, A. L., "Leading-edge vortices in insect flight," 1996.

[22]Birch, J. M. and Dickinson, M. H., "Spanwise flow and the attachment of the leading-edge vortex on insect wings," *Nature*, Vol. 412, No. 6848, 2001, pp. 729–733.

[23]Rossow, V. J., "Two-fence concept for efficient trapping of vortices on airfoils," *Journal of aircraft*, Vol. 29, No. 5, 1992, pp. 847–855.

[24]Iollo, A. and Zannetti, L., "Optimal control of a vortex trapped by an airfoil with a cavity," *Flow, turbulence and combustion*, Vol. 65, No. 3-4, 2000, pp. 417–430.

[25]Shi, S., New, T., and Liu, Y., "On the flow behaviour of a vortex-trapping cavity NACA0020 aerofoil at ultra-low Reynolds number," .

[26]Leishman, J. G., "Unsteady lift of a flapped airfoil by indicial concepts," *Journal of Aircraft*, Vol. 31, No. 2, 1994, pp. 288–297.

[27]Rennie, R. and Jumper, E. J., "Experimental measurements of dynamic control surface effectiveness," *Journal of aircraft*, Vol. 33, No. 5, 1996, pp. 880–887.

[28]Nguyen, K., "Active control of helicopter blade stall," *Journal of aircraft*, Vol. 35, No. 1, 1998, pp. 91–98.

[29]Feszty, D., Gillies, E. A., and Vezza, M., "Alleviation of airfoil dynamic stall moments via trailing-edge flap flow control," *AIAA journal*, Vol. 42, No. 1, 2004, pp. 17–25.

[30]Lee, T. and Gerontakos, P., "Dynamic stall flow control via a trailing-edge flap," *AIAA journal*, Vol. 44, No. 3, 2006, pp. 469–480.

[31]Gerontakos, P. and Lee, T., "PIV study of flow around unsteady airfoil with dynamic trailing-edge flap deflection," *Experiments in fluids*, Vol. 45, No. 6, 2008, pp. 955–972.

[32]Pope, A. and Harper, J. J., "Low Speed Wind Tunnel Testing John Wiley & Sons," *New York*, 1966.

[33]Kussner, H. and Schwartz, I., "The oscillating wing with aerodynamically balanced elevator," 1941.

[34]Theodorsen, T., "General Theory of Aerodynamic Instability and the Mechanism of Flutter," Tech. Rep. 496, NACA, 1935.

[35]Laitone, E., "Wind Tunnel Tests of Wings at Reynolds Numbers Below 70000," *Experiments in Fluids*, Vol. 23, 1997, pp. 405–409.

[36]Alam, M. M., Zhou, Y., Yang, H., Guo, H., and Mi, J., "The ultra-low Reynolds number airfoil wake," *Experiments in fluids*, Vol. 48, No. 1, 2010, pp. 81–103.